OPEN ACCESS

University of BRISTOL

Extending the Scope of "Living" Crystallization-Driven Self-Assembly: Well-Defined 1D Micelles and Block Comicelles from Crystallizable Polycarbonate Block Copolymers

John R. Finnegan,[1,4] Xiaoming He,[1,2] Steven T. G. Street,[1] J. Diego Garcia-Hernandez,[1] Dominic W. Hayward,[1] Robert L. Harniman,[1] Robert M. Richardson,[3] George R. Whittell[1] and Ian Manners[*1,4]

[1]School of Chemistry, University of Bristol, Bristol BS8 1TS, United Kingdom

[2]School of Chemical Science and Engineering, Tongji University, Shanghai

[3]HH Wills Physics Laboratory, Tyndall Avenue, Bristol BS8 1TL

[4]Department of Chemistry, University of Victoria, Victoria, BC V8W 3V6, Canada

ABSTRACT: Fiber-like block copolymer (BCP) micelles offer considerable potential for a variety of applications, however, uniform samples of controlled length and with spatially tailored chemistry have not been accessible. Recently, a seeded growth method, termed 'living' crystallization-driven self-assembly (CDSA), has been developed to allow the formation of 1D micelles and block comicelles of precisely controlled dimensions from BCPs with a crystallizable segment. An expansion of the range of core forming blocks that participate in living CDSA is necessary for this technique to be compatible with a broad range of applications. Few examples currently exist of well-defined, water-dispersible BCP micelles prepared using this approach, especially from biocompatible and biodegradable polymers. Herein, we demonstrate that BCPs containing a crystallizable polycarbonate, poly(spiro[fluorene-9,5'-[1,3]dioxin]-2'-one) (PFTMC), can readily undergo living CDSA processes. PFTMC-*b*-poly(ethylene glycol) (PEG) BCPs with PFTMC:PEG block ratios of 1:11 and 1:25 were shown to undergo living CDSA to form near monodisperse fiber like micelles of precisely controlled lengths of up to ~1.6 μm. Detailed structural characterization of these micelles by TEM, AFM, SAXS and WAXS, revealed that they comprise a crystalline, chain folded PFTMC core with a rectangular cross-section that is surrounded by a solvent swollen PEG corona. PFTMC-*b*-PEG fiber-like micelles were shown to be dispersible in water to give colloidally stable solutions. This allowed an assessment of the toxicity of these structures towards WI-38 and HeLa cells. From these experiments, we observed no discernable cytotoxicity from a sample of 119 nm fiber-like micelles to either the healthy (WI-38) or cancerous (HeLa) cell types. The living CDSA process was extended to PFTMC-*b*-poly(2-vinylpyridine) (P2VP), and addition of this BCP to PFTMC-*b*-PEG seed micelles led to the formation of well-defined segmented fibers with spatially localized coronal chemistries.

INTRODUCTION

The self-assembly of amphiphilic block copolymers (BCPs) in solution has been shown to yield a diverse range of nanoparticle morphologies.[1–3] Of these, high aspect ratio fiber-like (1D) micelles are particularly attractive, for example, in fields such as device fabrication and nanomedicine.[4–6] Whilst 1D worm- and rod-like micelles can be prepared from amorphous BCPs, this is typically limited to a narrow range of polymer block ratios and self-assembly conditions. Furthermore, samples are often contaminated by other morphologies.[1,7] In contrast, BCPs with a crystallizable core-forming block have generally been found to favor the formation of micelle morphologies with low curvature of the core-corona interface, such as fibers and platelets.[3,8,9] Thus, a wide range of polydisperse fiber-like BCP micelles with different crystalline core chemistries has now been shown to be accessible via a process termed crystallization-driven self-assembly (CDSA).[3,9–15]

The ability to control the length of fiber-like BCP micelles is also highly desirable as their dimensions are likely to affect

their behavior and performance in various applications. For example, in the case of optoelectronic device fabrication, the overall charge carrier mobility in nonwoven matts of semiconducting fibers should be length dependent.[16,17] Furthermore, in nanomedicine, the circulation time and clearance mechanism for rod-like drug delivery vehicles has been shown to be dependent on particle length.[6,18,19] In collaboration with Winnik and coworkers, we have previously demonstrated that sonication of polydisperse fiber-like micelles formed by CDSA via spontaneous nucleation yields small fragments or seeds, that function as "initiators" on the addition of further BCP which grows epitaxially from the seed termini (Scheme 1).[20–22] This yields low dispersity fibers of a length controlled by the ratio of added BCP to seed micelles.[22] Due to the analogy between this process and living covalent polymerizations, this process is termed 'living' CDSA.[22] Variants on the seed generation process are also possible. For example, small seeds can be formed by BCP self-assembly under conditions in which homogenous nucleation is favored[23] or, alternatively, in situ by thermal treatment and/or by using conditions of controlled solvency,[24] a method termed

"self-seeding" which has its origins in early work on the growth of polymer single crystals.[25]

Living CDSA has been extensively developed using BCPs containing poly(ferrocenyldimethylsilane) (PFS) as the crystallizable core-forming block.[26] With these materials it has been demonstrated that near monodisperse fiber-like micelles can be prepared with lengths varying from ~20 nm to greater than 5 μm.[22,27] In another demonstration of the powerful potential utility of living CDSA, block comicelles, random comicelles, and gradient comicelles can be prepared by combining unimers and seed micelles with a common core-forming block but chemically different corona-forming blocks.[27–30] Living CDSA can also be applied to PFS BCPs to prepare well-defined amphiphilic micelles which can subsequently be used as building blocks for hierarchical self-assembly.[31,32] The scope of living CDSA has also been expanded through the use of a growing range of BCPs and π-stacking molecular building blocks to permit the controlled fabrication of colloidally stable fibers with various chemistries and properties.[5,23,33–46]
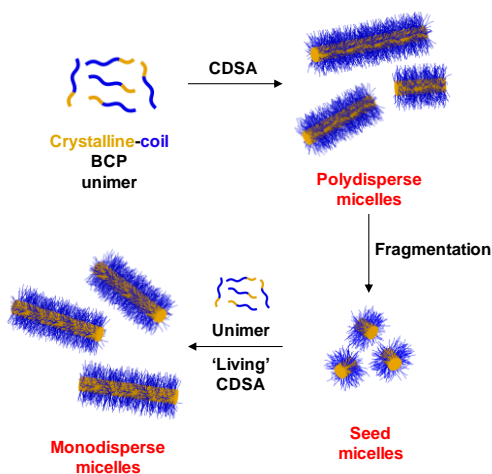

Scheme 1. Schematic representation of the preparation of monodisperse cylindrical micelles by living CDSA.

The ability to precisely create water-soluble high aspect ratio nanoparticles with complex coronal chemistries via living CDSA offers significant potential in the rapidly developing field of targeted drug delivery.[6,19,47] Furthermore, living CDSA should allow polymers with corona-forming blocks containing therapeutic, diagnostic and targeting functional groups to be combined within the same nanoparticle, allowing for facile customization of drug delivery vehicles. However, the preparation of water dispersible micelles from BCPs by living CDSA has to date scarcely been reported in the literature.[34,48] Whilst water-dispersible micelles with a PFS core can be prepared,[48] a crystallizable block with a biodegradable backbone would ultimately be better suited to in vivo applications. The polyesters poly(L-lactide) (PLLA) and poly(ε-caprolactone) (PCL) are crystalline materials that display desirable biocompatibility and biodegradability. Although the formation of water-soluble BCP micelles with crystalline cores comprised of each polymer has been demonstrated,[49–52] currently only PCL containing BCPs are capable of forming fiber-like micelles that are colloidally stable in water by a controlled seeded growth approach. Thus, in an important recent advance, Dove, O'Reilly and coworkers reported the formation of near monodisperse fiber-like micelles

of average lengths of up to 800 nm with a crystalline PCL core and a water-soluble corona.[34] Moreover, after preparing seed micelles in ethanol and transferring them by dialysis into water, living CDSA could even be carried out in an essentially aqueous environment.

Aliphatic polycarbonates have also emerged as a desirable class of polymers from which to fabricate medical devices for use in vivo because of their low inherent toxicity and biodegradability.[50] Of the synthetic aliphatic polycarbonates presented in the literature, poly(trimethylene carbonate) (PTMC) and its derivatives have been studied most extensively. Due to its hydrophobicity and low glass transition temperature ($T_g = -20$ ºC), PTMC has found use for the creation of soft implants/scaffolds and as the hydrophobic domain in micellar drug-delivery vehicles.[53–57] Under in vivo conditions polycarbonates are expected to undergo a different degradation mechanism to polyesters, such as PLLA and PCL, which are known to undergo bulk hydrolytic degradation resulting in the formation of acidic products capable of inducing an immune response and catalyzing further degradation of the polymer backbone.[58] Whereas hydrophobic polycarbonates have been shown to degrade more slowly via a surface erosion process to yield less harmful products (alcohols and CO_2).[59] These differences maybe be advantageous for the in vivo application of polycarbonate-core micelles, as slower degradation is expected to lead to longer circulation times and more benign degradation products should reduce the likelihood of unwanted side-effects.

High molar mass and low molar-mass dispersity ($Đ_M$) PTMC homopolymers and PTMC-containing BCPs can be prepared via living ring-opening polymerization (ROP) using metal-free organocatalysts (Scheme 2).[60] Recently, Hedrick, Yan Yang and coworkers described the synthesis of a series of diBCPs comprised of a poly(ethylene glycol) (PEG) block and a PTMC based coblock incorporating spirocyclic fluorenes, namely poly(spiro[fluorene-9,5'-[1,3]dioxin]-2'-one) (PFTMC).[61] These researchers also demonstrated that PFTMC-*b*-PEG BCPs were capable of forming water-soluble tape-like and/or spherical micelles upon dialysis from THF into water. The formation of tape-like micelles suggested that crystallization of the PFTMC block had occurred during self-assembly. This prompted the studies reported herein, where we demonstrate that PFTMC-*b*-PEG BCPs are able to undergo living CDSA to form water-dispersible fiber-like micelles of precisely controlled length. This work represents the first example of living CDSA using a polycarbonate core-forming block.
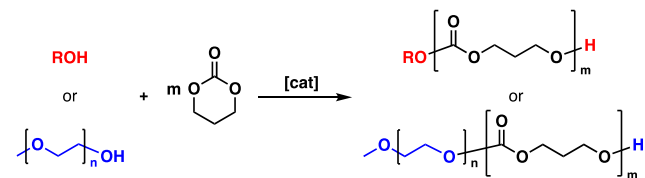
Scheme 2. Synthesis of PTMC homopolymer and the BCP PTMC-*b*-PEG by ROP.

RESULTS

Crystallization Behavior of PFTMC Homopolymer. The crystallinity of PFTMC is a prerequisite for its role as a core-forming block in CDSA, however the ability of this material to crystallize has not previously been demonstrated. To explore the potential crystallization of PFTMC, a sample of homopolymer was therefore synthesized using a procedure adapted from
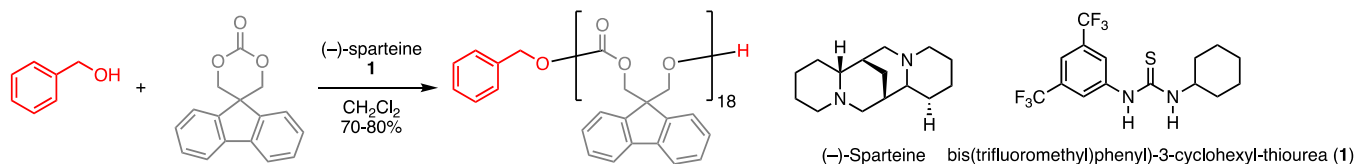
Scheme 3. Synthesis of PFTMC$_{18}$ homopolymer via organocatalytic ROP.

**Table 1.** Summary of PFTMC-*b*-PEG BCP molecular weight data.

Polymer	PFTMC DP$_n$ [a]	PEG DP$_n$ [a]	Đ$_M$ [b]	PFTMC:PEG Block Ratio[a]	PFTMC:PEG Mass Ratio[a]
PFTMC$_{20}$-*b*-PEG$_{44}$	19	44	1.09	1:2	2.5:1
PFTMC$_{20}$-*b*-PEG$_{220}$	19	220	1.07	1:11	1:2.0
PFTMC$_{20}$-*b*-PEG$_{490}$	18	490	1.08	1:25	1:4.8

[a] determined by ^{1}H NMR spectroscopy, [b] determined by GPC relative to PS standards.

the work of the Waymouth, Hedrick and Yang groups, as shown in Scheme 3.[60,61] ROP of the cyclic carbonate, spiro[fluorene-9,5'-[1,3]dioxin]-2'-one (FTMC), was initiated in anhydrous CH$_2$Cl$_2$ at 23 ºC by benzyl alcohol in the presence of two organic catalysts, (–)-sparteine and 1-(3,5-bis(trifluoromethyl)phenyl)-3-cyclohexyl-thiourea (**1**). The role of **1** is to activate the carbonyl group of the FTMC monomer towards nucleophilic attack, whereas the role of (–)-sparteine is to increase the nucleophilicity of the initiating and propagating alcohol species present during the polymerisation.[62] This catalytic system has been shown to yield low dispersity PTMC homopolymers with excellent end-group fidelity by suppressing carbonate interchange reactions.[60] As a result, we were able to produce a well-defined PFTMC homopolymer with a number-average degree of polymerization (DP$_n$) of 18 and a Đ$_M$ of 1.05, as determined by matrix-assisted laser desorption/ionization time of flight mass spectrometry (MALDI-TOF MS) and gel permeation chromatography (GPC) respectively (Figure S1 and S2). The crystallization behavior of the polymer sample was subsequently investigated by a combination of differential scanning calorimetry (DSC) and wide-angle X-ray scattering (WAXS). DSC revealed a glass transition temperature of 119 ºC and two first-order endothermic transitions, one at 153 ºC and another at 171 ºC, either side of a small exothermic transition (Figure S3). We attribute these transitions to a structural reorganization during the DSC scan. First, small crystalline domains melt at 153ºC producing the first endotherm which is followed by an exothermic transition corresponding to reorganization of the polymer chains to form larger crystalline domains which eventually melt at 171ºC. Similar thermal behavior has been observed for other semi-crystalline polymers such PFS and polyethylene (PE).[63,64] After annealing a PFTMC film at 140 ºC on a Kapton substrate, seven peaks including four first-order reflections could be observed in the WAXS diffraction pattern (Figure S4). The reflections could be indexed to an orthorhombic unit cell with the parameters a = 15.4, b = 5.7 and c = 4.1 Å (for further details see Supporting Information).

Synthesis and Self-Assembly of PFTMC-*b*-PEG Block Copolymers. To investigate the effect of block ratio on the CDSA of PFTMC-*b*-PEG polymers, a series of BCPs was prepared using different molecular weight mono-hydroxyl PEG macroinitiators. PEG$_{490}$, PEG$_{220}$ and PEG$_{44}$ were used to initiate the ROP of FTMC in anhydrous CH$_2$Cl$_2$ as shown in Scheme 4,

and in each case a PFTMC block with a DP$_n$ of 20 was targeted. For the synthesis of PFTMC$_{20}$-*b*-PEG$_{44}$ and PFTMC$_{20}$-*b*-PEG$_{220}$, (+)-sparteine and **1** were used as the ROP catalysts. However, for the synthesis of PFTMC$_{20}$-*b*-PEG$_{490}$ a more active catalyst, 1,8-diazabicyclo[5.4.0]undec-7-ene (DBU), was required to reach a PFTMC monomer conversion of >80%. Like the use of (–)-sparteine and **1**, DBU can catalyze the ROP of TMC, but at significantly lower catalyst loading. This catalyst has also been shown to achieve high degrees of monomer conversion without molecular scrambling of the polymer chain ends occurring.[60] For each BCP, the DP$_n$ of the PFTMC segment was determined using ^{1}H NMR spectroscopy by comparing the relative integrals of the peaks from methylene groups of PFTMC at 4.28-4.48 ppm, and the singlet at 3.40 ppm from the methyl end group of the PEG block (Figure S5). To ensure controlled BCP self-assembly it was important to remove any PFTMC homopolymer that may have been generated during the BCP synthesis. As the fluorene moiety in PFTMC absorbs strongly at 240 nm, it could be easily detected by monitoring UV absorbance of eluting fractions separated by GPC. PFTMC homopolymer was removed via selective precipitation resulting in pure PFTMC$_{20}$-*b*-PEG$_n$ BCPs. This was confirmed by the absence of any low molecular weight shoulder in the GPC traces of each BCP and by ^{1}H-DOSY NMR spectroscopic analysis, which showed no peaks corresponding to the diffusion of PFTMC$_{20}$ homopolymer (Figure S6 and S7). The molecular weight characterization of all three polymers is summarized in Table 1.
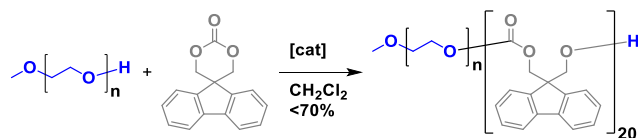
Scheme 4. Synthesis of PFTMC$_{20}$-*b*-PEG$_n$ (n = 44, 220, 490) via organocatalytic ROP. (–)-sparteine and 1 were used as the catalysts for the preparation of PFTMC$_{20}$-*b*-PEG$_{44}$ and PFTMC$_{20}$-*b*-PEG$_{220}$. DBU was used as the catalyst for the preparation of PFTMC$_{20}$-*b*-PEG$_{490}$.

Initially, the solution state self-assembly behavior of PFTMC$_{20}$-*b*-PEG$_{490}$, PFTMC$_{20}$-*b*-PEG$_{220}$ and PFTMC$_{20}$-*b*-PEG$_{44}$ was investigated by attempting to form micelles via spontaneous nucleation in mixtures of MeOH and
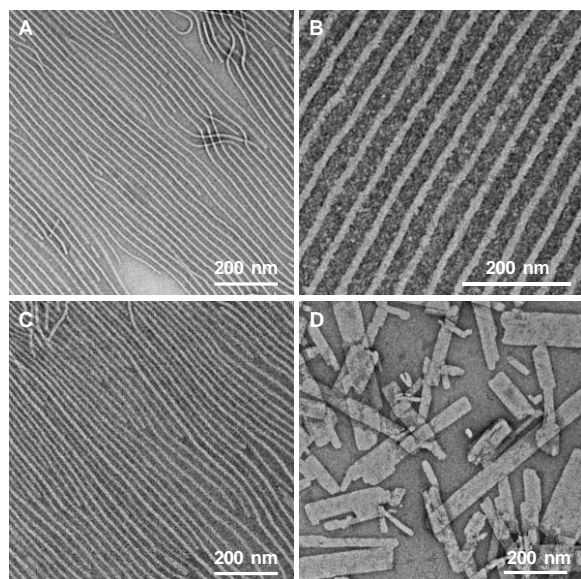
Figure 1. TEM images of micelles prepared via spontaneous nucleation in mixtures of MeOH and DMSO by heating polymer samples to 70 °C before cooling to 23 °C over a period of 2.5 h. A and B) PFTMC$_{20}$-*b*-PEG$_{490}$ (MeOH:DMSO (v:v) 9:1, 0.5 mg/mL). C) PFTMC$_{20}$-*b*-PEG$_{220}$ (MeOH:DMSO (v:v) 4:1, 0.2 mg/mL). D) PFTMC$_{20}$-*b*-PEG$_{44}$ (MeOH:DMSO (v:v) 3:2, 0.05 mg/mL, sample sonicated for 1 minute prior to imaging to improve sample dispersion on the TEM substrate). TEM samples were stained with a 3 wt% solution of uranyl acetate in EtOH.

DMSO (Figure 1). Under these conditions, MeOH acts as selective solvent for the PEG blocks, promoting self-assembly via solvophobic interactions between the PFTMC blocks, whereas a small amount DMSO acts as a common solvent for both blocks, presumably promoting PFTMC plasticization and crystallisation.[65] PFTMC$_{20}$-*b*-PEG$_{490}$ micelles were prepared by annealing the BCP at 0.5 mg/mL in 9:1 MeOH:DMSO (v:v) at 70 °C for 8 h before cooling to 23 °C over a period of 2.5 h. PFTMC$_{20}$-*b*-PEG$_{220}$ micelles were prepared via the same annealing and cooling procedure in 4:1 MeOH:DMSO (v:v) at a concentration of 0.2 mg/mL. The morphology of the resulting micelles was analyzed by TEM after application of a uranyl acetate stain (3 wt% in EtOH). The stain solution was selected to increase the contrast of the PFTMC$_{20}$-*b*-PEG$_n$ micelles which because of their low electron density, are otherwise difficult to visualize by TEM. As EtOH is a moderate solvent for PEG it is expected that the stain solution will coat the carbon film and penetrate the micelle corona, leaving only the areas of the film covered by the micelle cores unstained. Thus, we expected the micelle cores to appear bright against a dark background when imaged by TEM. In both the case of PFTMC$_{20}$-*b*-PEG$_{490}$ and PFTMC$_{20}$-*b*-PEG$_{220}$ exclusively fiber-like micelles were observed by TEM (Figure 1A-C and Figure S8). These micelles appear uniform in width but are polydisperse in length, with lengths predominantly greater than 5 µm. Micelles prepared from PFTMC$_{20}$-*b*-PEG$_{490}$ had a number average width (W_n) of 17 nm with a standard deviation of 3 nm and the micelles prepared from PFTMC$_{20}$-*b*-PEG$_{220}$ had a W_n of 15 nm with a standard deviation of 2 nm. When PFTMC$_{20}$-*b*-PEG$_{44}$ was annealed in a sealed vial at 70 °C in 3:2 MeOH:DMSO (v:v) at

0.05 mg/mL for 8 h, then cooled to 23 °C, this resulted in a turbid suspension which was briefly (~1 min) sonicated to better disperse any large aggregates prior to TEM analysis. This revealed predominantly rectangular shaped micelles irregular in length and with widths ranging from 20 to greater than 200 nm (Figure 1D and S9). Further studies of these 2D PFTMC$_{20}$-*b*-PEG$_{44}$ micelles will be carried out in the future as in this manuscript we focus on 1D assemblies.

Living CDSA of PFTMC-*b*-PEG Block Copolymers. Seed micelles were prepared from the polydisperse PFTMC$_{20}$-*b*-PEG$_{490}$ and PFTMC$_{20}$-*b*-PEG$_{220}$ micelles by sonication for 2 h at 15 °C (Figure 2A). The seed micelles prepared from PFTMC$_{20}$-*b*-PEG$_{490}$ had a number average length (L_n) of 40 nm and an apparent width of ~23 nm. The dispersity in length was low, with L_w/L_n equal to 1.10 (where L_w corresponds to weight average length). Interestingly, closer inspection of the seed micelles appeared to show two populations of micelles that differed in width, with the widths of the two populations centering on 19 and 27 nm (Figure 2B-C). To characterize the dimensions of these micelles further, they were analyzed by AFM. This revealed that the population of micelles with a greater width had a height of ~6 nm and the narrower micelles had a height of ~10 nm (Figure 2D and E). This data, combined with the TEM analysis, strongly indicates the PFTMC$_{20}$-*b*-PEG$_{490}$ seed micelles have an approximately rectangular cross-section, and that the bimodal distribution of micelle widths observed by TEM is a result of micelles lying on their largest face or on their edge. Furthermore, the increase in apparent average width of these seeds compared to their polydisperse precursors implies that with increasing length PFTMC$_{20}$-*b*-PEG$_{490}$ micelles are less likely to lie on their largest face.
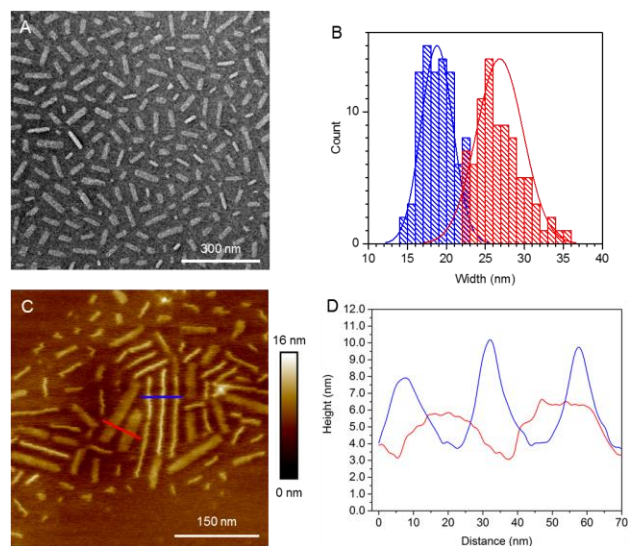

Figure 2. A) TEM image of PFTMC$_{20}$-*b*-PEG$_{490}$ seed micelles. Sample stained with a 3 wt% solution of uranyl acetate in EtOH. B) Histogram of PFTMC$_{20}$-*b*-PEG$_{490}$ seed micelle widths showing a bimodal distribution. C) AFM height image of PFTMC$_{20}$-*b*-PEG$_{490}$ seed micelles. D) Linear height profiles from C).
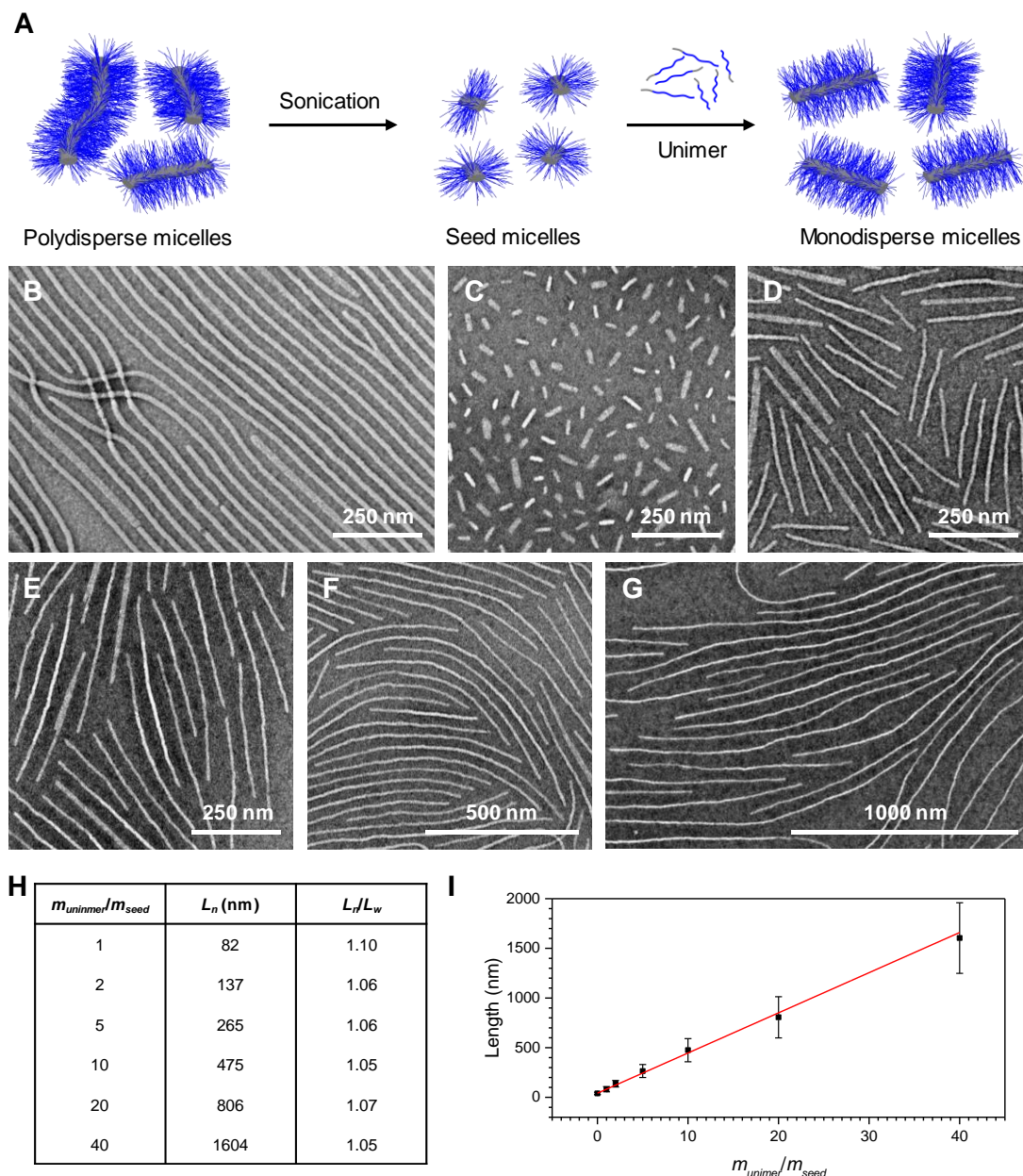
Figure 3. A) Schematic representation of the preparation of monodisperse PFTMC$_{20}$-b-PEG$_{490}$ micelles. TEM images of PFTMC$_{20}$-b-PEG$_{490}$ micelles prepared by self-nucleation (B), PFTMC$_{20}$-b-PEG$_{490}$ seed micelles (C) and monodisperse PFTMC$_{20}$-b-PEG$_{490}$ micelles prepared by the addition of 5 (D), 10 (E), 20 (F) and 40 (G) mass equivalents of unimer. Samples were stained with a 3 wt% solution of uranyl acetate in EtOH. H) Micelle length summary. I) Plot of m_{unimer}/m_{seed} against L_n, slope = 40 nm/equivalent unimer added.

Monodisperse fiber-like PFTMC$_{20}$-b-PEG$_{490}$ micelles of precisely controlled length were prepared via seeded growth by adding a solution of unimeric PFTMC$_{20}$-b-PEG$_{490}$ in DMSO to solutions of seed micelles (L_n = 40, L_w/L_n = 1.10) in MeOH:DMSO (≥90% MeOH by volume). Samples prepared with unimer to seed mass ratios (m_{unimer}/m_{seed}) of 1, 2, 5, 10, 20 and 40 resulted in micelles with L_n (and L_w/L_n) values of 82 (1.10), 137 (1.06), 265 (1.06), 475 (1.06), 806 (1.07) and 1604 nm (1.05) respectively (Figure 3), and a linear trend in the relationship between micelle length and m_{unimer}/m_{seed} was observed (Figure 3I). Assuming each micelle end remains active throughout the growth process, complete conversion of added unimer, a constant number of BCPs per unit length ($N_{agg,L}$) and the absence of spontaneous nucleation, each equivalent of unimer

added should increase the length of the resulting micelles by the same value as the length of the seed micelles. Fitting a straight line to the plot of m_{unimer}/m_{seed} against L_n gives a slope with a gradient of 40 nm/equivalent of unimer (Figure 3I) which is in good agreement with the experimentally determined value, suggesting that the previously mentioned assumptions about the micelle growth process hold true for this system. Micelle length characterization is summarized in Table S3 and histogram highlighting the narrow length distributions are shown in Figure S10.

Seed micelles were also prepared from PFTMC$_{20}$-b-PEG$_{220}$ and possessed a L_n of 40 nm (L_w/L_n = 1.17). Again, a bimodal distribution in micelle width was observed by TEM which can

5

also likely be attributed to drying of the seed micelles in two different orientations (Figure S11). $PFTMC_{20}\text{-}b\text{-}PEG_{220}$ fiber-like micelles of precisely controlled length were then prepared by the addition of unimer to seed solutions. A linear relationship was observed between micelle length and m_{unimer}/m_{seed} and the gradient of the linear fit was 38 nm (Figure S12). This value is again in good agreement with the theoretical value based on the criteria outlined earlier and the length of the seed micelles. This confirmed complete conversion of unimer to micelle, the absence of spontaneous nucleation, and a constant $N_{agg,L}$ during self-assembly. Micelle length characterization is summarized in Table S4 and histograms highlighting the narrow length distributions are shown in Figure S13.

Colloidal Stability of $PFMC_{20}\text{-}b\text{-}PEG_{490}$ Micelles in Water. To explore the colloidal stability of fiber-like PFTMC-b-PEG micelles in water, first a 0.2 mg/mL (MeOH:DMSO, 4:1 (v:v)) colloidal solution of $PFTMC_{20}\text{-}b\text{-}PEG_{490}$ micelles prepared by spontaneous nucleation was dialyzed against water. This resulted in a clear, stable colloidal solution and no change in micelle morphology was detectable by TEM analysis (Figure S14). Following this, low length dispersity $PFTMC_{20}\text{-}b\text{-}PEG_{490}$ micelles with a L_n of 40 and of 540 nm were prepared separately in MeOH:DMSO and dialyzed into water (Figure 4 and S15). In both cases this resulted in a clear colloidal solution of micelles with no obvious precipitation. To assess the stability of these fiber-like micelles in water the colloidal solutions were aged for 2 weeks and the micelles analyzed again by TEM. It was observed that the micelles retained their fiber-like structure and showed no signs of aggregation or degradation. Furthermore, the L_n of the micelles measured before and after dialysis were in close agreement and no significant increase in L_w/L_n was observed.

In an attempt to carry out living CDSA in water, $PFTMC_{20}\text{-}b\text{-}PEG_{490}$ unimer (10 mg/mL in DMSO) equivalent to a m_{unimer}/m_{seed} ratio of 10 was added to the aqueous solution of 40 nm $PFTMC_{20}\text{-}b\text{-}PEG_{490}$ seed micelles. TEM analysis revealed what appeared to be mixture of the original seed micelles and a large excess of spherical micelles (Figure S16A). It appears that added unimer initially contributes to little or no growth from the seed micelles and instead, the added polymer is converted to spherical micelles. This prompted us to add a unimer solution directly into water in an attempt to form a pure solution of spherical micelles. TEM analysis of this solution revealed micelles with an exclusively spherical morphology and an average diameter of 15 nm (Figure S16B). WAXS analysis of a 20 mg/mL solution of spherical $PFTMC_{20}\text{-}b\text{-}PEG_{490}$ micelles in water:DMSO 4:1 (v:v) revealed no Bragg peaks (Figure S16C). Later in this work we discuss the presence of Bragg peaks in the scattering pattern of a 16 mg/mL solution of fiber-like $PFTMC_{20}\text{-}b\text{-}PEG_{220}$ micelles. Therefore, the absence of these reflections in this instance, indicates that the PFTMC core of the spherical micelles is in an amorphous state. However, it also possible that crystalline domains of PFTMC exist in the sample which are too small to produce detectable Bragg peaks.
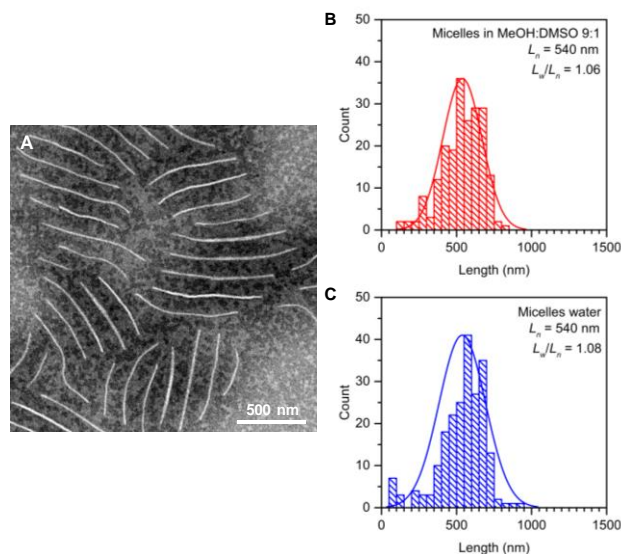

Figure 4. A) TEM image of $PFTMC_{20}\text{-}b\text{-}PEG_{490}$ micelles after dialysis from MeOH:DMSO into water. TEM samples were stained with a 3 wt% solution of uranyl acetate in EtOH. Contour length histograms from micelles measured before dialysis (B) and after dialysis (C).

To investigate the temporal stability of $PFTMC_{20}\text{-}b\text{-}PEG_{490}$ spherical micelles, the samples prepared with and without seeds were aged at 23 ºC in sealed vials. After 30 days, TEM analysis of the sample containing both seed and spherical micelles showed the presence of a small percentage (<5%) of fiber-like micelles greater than 100 nm in length, with the majority of the sample retaining the original spherical morphology (Figure S17A). After 60 days, the sample that previously contained only spherical micelles was analyzed by TEM and shown to contain a large population of fiber-like micelles greater than 500 nm in length, numerous shorter fiber-like micelles and spherical micelles could also be observed by TEM (Figure S17B). These results show that slow conversion from spherical to fiber-like micelles takes place in an aqueous environment, likely via a processes driven by crystallization of the micelle cores, as has previously been observed in the study of PFS and PE containing BCP self-assembly.[12,66,67]

Assessing the Cytotoxicity of Fiber-Like PFTMC-b-PEG Micelles. To examine the potential biocompatibility of PFTMC-b-PEG micelles, 24 h cytotoxicity assays were conducted using a combined calcein AM (to assess cell viability) and alamarBlue (to assess reductive metabolism) assay. $PFTMC_{20}\text{-}b\text{-}PEG_{490}$ fiber-like micelles were prepared with a L_n of 119 nm ($L_w/L_n = 1.04$) and were incubated with primary WI-38 fetal lung fibroblasts and HeLa cervical cancer cells at concentrations ranging from 1-100 µg/mL. Micelles with a length of 119 nm were chosen because rod-like nanoparticles of this size are thought to be especially desirable for drug delivery applications, as they are likely to exhibit a long circulation half-life within the body.[6,18] Analysis of the resulting cell populations showed that at every concentration of $PFTMC_{20}\text{-}b\text{-}PEG_{490}$ examined (up to 100 µg/mL), there was no statistically significant reduction in cell viability in either cell line, while cellular metabolism was unaffected for primary WI-38 cells and remained above 86% for the HeLa cell line (Figure 5 and S18).

Table 2. Dimensions of PFTMC20-b-PEG220 micelles prepared at 8 mg/mL in MeOH:THF (4:3) as determined by TEM, AFM and SAXS (analyzed after diluting to 4 mg/mL).

Technique	Length (nm)	Core height (nm)	Core width (nm)	Corona thickness (nm)	$N_{agg,L}$ (molecules/nm)
AFM	–	6	15	–	–
TEM	530	–	16	–	–
SAXS (Model 2)[a]	–	5	21	11	17

[a] Micelle core dimensions determined by refining the model to fit in the range 0.004> Q <0.1.
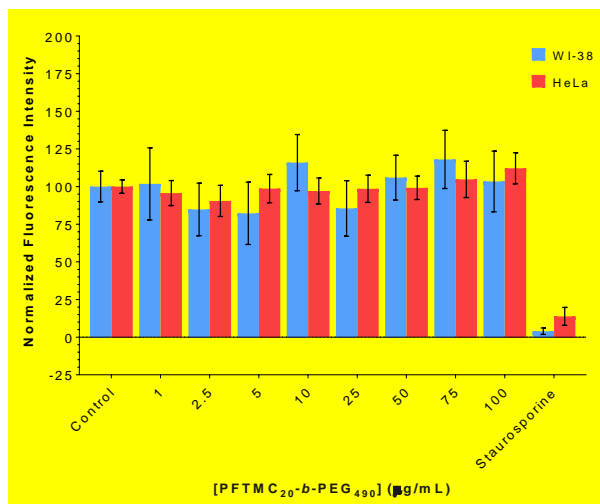

Figure 5. Biocompatibility of fiber-like PFTMC$_{20}$-b-PEG$_{490}$ micelles (L_n = 119 nm, L_w/L_n = 1.04) with WI-38 and HeLa cells measured after 24 exposure in a calcein AM assay. No statistically significant change in cell viability was observed at any concentration up to 100 µg/mL. For the effects of PFTMC$_{20}$-b-PEG$_{490}$ micelles on cell metabolism, see Supporting Information. Data was averaged over three repeat experiments, and errors are represented as the 95% confidence interval.

To further probe the cytotoxicity of PFTMC-b-PEG micelles, we also examined the effect of 9H-fluorene-9,9-dimethanol, the hydrolysis product of PFTMC, on WI-38 and HeLa cells.[61] IC$_{50}$ values for 9H-fluorene-9,9-dimethanol were calculated for both cell types, with IC$_{50}$ values for cell mortality of 0.45 mM and 1.01 mM for WI-38 and HeLa cells respectively, and IC$_{50}$ values for reductive metabolism of 0.38 mM for WI-38 cells and 0.80 mM for HeLa cells (Figure S19, see Supporting Information for further details). These concentrations are much higher than are commonly encountered for many small molecule cytotoxic agents, and the authors envisage that the cytotoxicity of 9H-fluorene-9,9-dimethanol should not present a barrier to the vast majority of nanomedicine applications. It should be noted that large, needle-like crystals were observed by optical microscopy at concentrations >100 µg/mL of 9H-fluorene-9,9-dimethanol, which might disrupt the extracellular matrix of the cells, resulting in the observed cytotoxicity (Figure S20).

X-Ray Scattering Characterization of Fiber-Like PFTMC-b-PEG Micelles. To probe the structure of the crystalline core of fiber-like PFTMC-b-PEG micelles, concentrated colloidal solutions of fiber-like PFTMC$_{20}$-b-PEG$_{220}$ micelles (L_n = 533 nm, L_w/L_n = 1.03) were prepared and analyzed by small-angle X-ray scattering (SAXS). Following application of a correction for solvent scattering and the scattering from an

empty capillary tube the data was analyzed. Based on the structure factors for samples with concentrations of 8, 12 and 16 mg/mL, a micelle solution at 4 mg/mL (MeOH:THF (v:v) 4:3) appeared to be below the concentration limit for significant interparticle interactions (Figure S21). The log/log plot for I vs Q from this sample shows a gradient of approximately -1 when Q is less than 0.01 Å^{-1} and a gradient of close to -4 when Q is between 0.02 and 0.03 Å^{-1} consistent with a solution of infinitely dilute rods (Figure S22).[68,69] To obtain further information about the cross-sectional structure of these micelles, two models for a solution of infinitely dilute rod-like nanoparticles were used to fit the data (Figure 6). Model 1 describes infinitely long micelles with a circular core cross-section surrounded by a circularly symmetrical corona (this model has previously been used to fit the scattering intensity from cylindrical micelles with a PFS core, Figure S23).[70] Whereas Model 2 is based on a description of fiber-like micelles with a crystalline core used by Vilgis and Halperin and describes the scattering intensity from micelles of infinite length with a rectangular core cross-section.[71] In this model for simplicity, coronal chains are confined solely to the two longest edges (Figure S24).[71] The details of Model 2 can be found in the Supporting Information. Nonlinear least-squares fits were conducted with both models by allowing the scaling factor, background, scattering-length density (SLD) of the corona near the core, along with the dimensions and polydispersity of the micelle core and corona cross-section to refine. The initial value for the SLD of the core was predicted using the literature value for the density of PFTMC.[72]
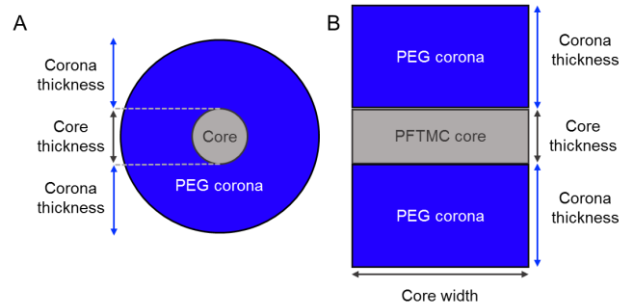
Figure 6. Schematic representation of the micelle cross-sections used to fit SAXS data. A) Model 1: a micelle with a circular core cross-section and a circularly symmetrical corona. B) Model 2: a micelle with a rectangular core cross-section and coronal chains confined to the two largest faces.

Both models afforded good fits for the observed scattering pattern for 0.004> Q <0.1 and limiting the fitting to this range did not allow for a distinction to be made. AFM analysis of the micelles was therefore used to determine which model was most appropriate. This revealed that the micelles are very uniform in

height along their length and have a uniform height of approximately 6 nm regardless of their width (Figure S25). This eliminates the possibility of a circular cross-section as core height would vary with core width if this were the case. AFM analysis also revealed that micelles above a certain length favor drying in a single orientation, unlike short seed micelles which were observed to lie on a surface in two different conformations. It is should be noted, however, that an ellipsoidal cross-section cannot be ruled out and resolving the subtle distinction between an elliptical and rectangular micelle cross-section is beyond the scope of this work. The width of the micelles prepared for SAXS analysis was measured by AFM, giving a value of 15 nm which is in good agreement with the value obtained from TEM analysis of 100 micelles, and close to that determined by fitting the SAXS data to Model 2 (Table 2). Having determined the core dimensions of the micelles (PFTMC$_{20}$-b-PEG$_{220}$, L_n = 530 nm) using SAXS and TEM enabled us to gain further into the overall micelle structure. Using the density of PFTMC (ρ = 1.33 g/cm^{-3}),[72] the volume of micelle core acquired from modelling the SAXS data, and the average mass of the PFTMC core-forming block, the number of polymer molecules comprising an average micelle was calculated to be ~9300, which equates to a $N_{agg,L}$ of 17. For a full description of how $N_{agg,L}$ was calculated see the Supporting Information section. Model 2 also provides information about the density of coronal chains at the core-corona interface through the predicted SLD of the corona, by comparison of the refined SLD for the corona with those known for PEG and the solvents used for self-assembly. The value for the former correlated strongly with the thickness of the coronal domains, and a good fit was obtained for a SLD of 8.29×10^{-5} Å^{-2} for a thickness of 10.5 nm which corresponds to a PEG volume fraction of 0.12±0.01 (See Supporting Information).

Concentrated micelle solutions were also studied by WAXS. From a 16 mg/mL sample, Bragg peaks at Q values of 0.410, 0.821 and 1.111 Å^{-1} can clearly be observed (Figure S26), which closely match the position of three peaks observed in the WAXS pattern of a PFTMC homopolymer film. The same peaks also form part of a series of reflections in the WAXS of a film prepared from the micelles (Q = 0.408, 0.823, 1.122, 1.237 and 1.911 Å^{-1}) (Figure S27). To determine the orientation of the PFTMC chains within the rectangular cross-section of the micelle core, molecular mechanics were used to determine the length of chain extended PFTMC oligomers with 5, 10, 15 and 20 repeat units (Figure S28). This revealed an average unit length per monomer of 0.54 nm. Therefore, the average chain length of the PFTMC$_{20}$ core-forming blocks corresponds to ~10.8 nm which is significantly less than the width of the micelle core and approximately twice the height. This suggests each chain is orientated parallel to the shortest axis of the micelle core and, on average, undergoes one chain fold as shown in Figure 7.
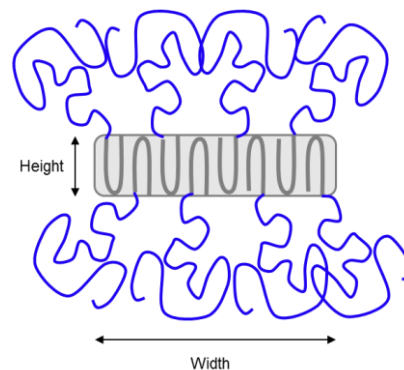

Figure 7. Schematic illustration of the cross-section of a fiber-like PFTMC$_{20}$-b-PEG$_{220/490}$ micelles. Core chains are orientated parallel to the height dimension of the core and on average undergo one chain fold. In accordance with the model outlined by Vilgis and Halperin, core-corona junction points are confined to the fold surfaces.[71] This is expected to result in a maximum PEG grafting density of on average 0.25 chains per PFTMC chain terminus.

Block Comicelles with a PFTMC Core. Finally, we aimed to extend the concept of living CDSA using BCPs with PFTMC core-forming block to include the formation of fiber-like micelles with a segmented coronal structure. To achieve this, first a BCP with a poly(2-vinylpyridine) (P2VP) corona-forming block was prepared via a two-step procedure (Scheme S1). The ROP of FTMC was initiated by 6-hydroxyhexyl-4-[(benzenecarbothioyl)sulfanyl]4-cyanopentanoate, a bifunctional reversible addition-fragmentation chain transfer agent (RAFT-CTA) that can been used to polymerize 2-vinylpyridine (2VP).[73] This yielded a PFTMC homopolymer (PFTMC$_{18}$-CTA) with a DP$_n$ of 18 ($Ð_M$ = 1.08) and ~60% CTA end-group functionality, as determined by MALDI-TOF MS and ^{1}H NMR spectroscopic analysis, respectively (Figures S29 and S30). PFTMC$_{18}$-CTA was then used to initiate the RAFT polymerization of 2VP, which, as a result of the presence of PFTMC chains without CTA end-group functionality, yielded a mixture of PFTMC$_{18}$-b-P2VP and PFTMC homopolymer. PFTMC$_{18}$-b-P2VP was then purified by selective precipitation of the BCP from THF via the addition of hexanes and BCP purity assessed by GPC and ^{1}H DOSY NMR. No peak with same retention time as PFTMC$_{18}$-CTA was observed in the GPC chromatogram, and no signals associated with either PFTMC or P2VP homopolymers observed in the 2D DOSY NMR spectrum indicating that pure PFTMC$_{18}$-b-P2VP had been isolated (Figure S31). By comparing the relative integrals of the methylene protons from PFTMC-CTA$_{18}$ at 4.4 ppm, with one of the aromatic protons from P2VP at 8.3 ppm, the DP$_n$ of the P2VP segment was determined to be 157 (Figure S32). BCP $Ð_M$ was measured by GPC and shown to be 1.21, the molecular weight data for both PFTMC$_{18}$-CTA and PFTMC$_{18}$-b-P2VP$_{157}$ is summarized in Table S2.

The self-assembly of PFTMC$_{18}$-b-P2VP$_{157}$ was studied using iPrOH as a selective solvent for P2VP, a solution of the BCP in THF (5 mg/mL) was added to a mixture of iPrOH and THF at 23 ºC to induce spontaneous micelle nucleation (final concentration 0.5 mg/mL, iPrOH:THF 7:3 v:v). TEM analysis of the resulting solution revealed the formation of length polydisperse fiber-like micelles (Figure S33A), similar to those produced by PFTMC$_{20}$-b-PEG$_{220/490}$. These fiber-like micelles were then sonicated for 2 h at 0 ºC to produce short monodisperse seed
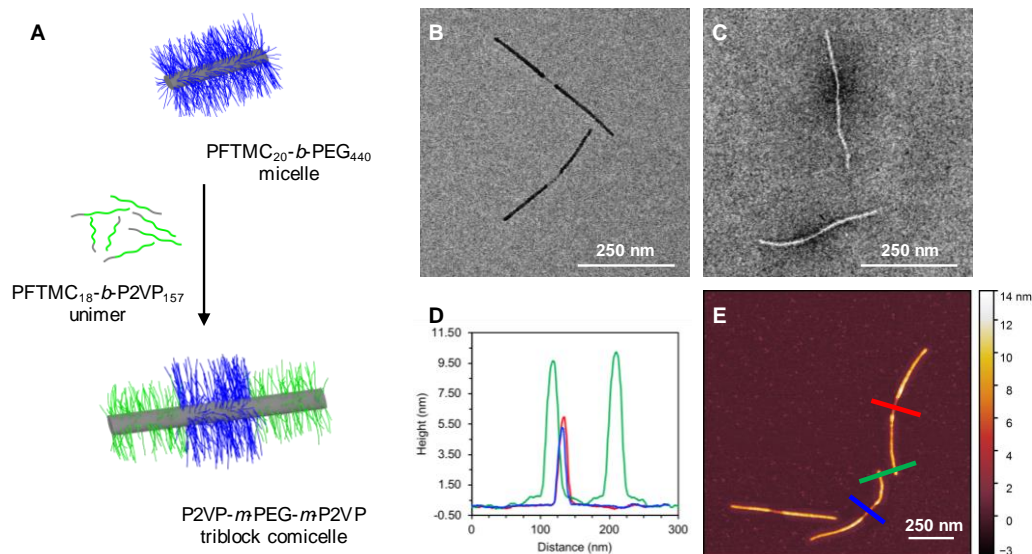
Figure 8. P2VP-*m*-PEG-*m*-P2VP block comicelles prepared from PFTMC$_{20}$-*b*-PEG$_{490}$ seeds (L_n = 60 nm, L_w/L_n = 1.10) and PFTMC$_{18}$-*b*-P2VP$_{157}$ unimer. A) Schematic representation of block comicelle preparation. B) TEM image of triblock comicelles without staining. C) TEM image of triblock comicelles after staining with 3 wt% uranyl acetate in EtOH. D) Linear height profiles from AFM height image of P2VP-*m*-PEG-*m*-P2VP micelles (E).

micelles with a L_n of 60 nm (L_w/L_n = 1.08) as determined by TEM (Figure S33B). Unlike PFTMC$_n$-*b*-PEG$_m$ micelles, which because of their low electron contrast require the addition of a negative stain prior to TEM imaging, PFTMC$_{18}$-*b*-P2VP$_{157}$ could clearly be observed by TEM without staining, due to the high electron contrast of the P2VP corona. Next, aliquots of a solution of PFTMC$_{18}$-*b*-P2VP$_{157}$ in THF, equivalent to different m_{unimer}/m_{seed}, were added to PFTMC$_{18}$-*b*-P2VP$_{157}$ seed micelles resulting in the formation of elongated fiber-like micelles of low length dispersity (Figure S34). The contour length data of these micelles is summarized in Table S6. It was demonstrated that micelles could be prepared with a L_n of greater than 2 μm, and that a linear fit could be applied to the relationship between L_n and m_{unimer}/m_{seed} (Figure S34B). The gradient of this fit is 55 nm/mass equivalent unimer which is in good agreement with the length of the seed micelles, indicating that PFTMC$_{18}$-*b*-P2VP$_{157}$ is capable of efficient living CDSA.

Due the good solubility of both PEG and P2VP in MeOH, it was anticipated that block comicelles could be prepared by adding PFTMC$_{18}$-*b*-P2VP$_{157}$ unimer to PFTMC$_{20}$-*b*-PEG$_{220}$ seed micelles in MeOH. PFTMC$_{18}$-*b*-P2VP$_{157}$ unimer (10 mg/mL in THF) was added to PFTMC$_{20}$-*b*-PEG$_{220}$ micelles with a L_n of 60 nm, resulting in symmetrical 1D triblock comicelles (P2VP-*m*-PEG-*m*-P2VP). The corona of the outer two segments of these micelles is composed of P2VP and the central segment of PEG. The difference in electron contrast between PEG and P2VP allowed the segmented structure to be clearly observed when drop cast samples were analyzed by TEM both with and without staining (Figure 8A and B), and the difference in corona height revealed the segmented structure when analyzed by AFM (Figure **8**C and D).

DISCUSSION

Effect of Block Ratio on PFTMC-*b*-PEG Micelle Morphology. Although the self-assembly behavior of PFTMC BCPs has previously been reported in the literature,[61] the structure of the resulting micelles has not been fully characterized,

nor has their assembly been precisely controlled. The presence of melt transitions in the DSC thermogram of PFTMC homopolymer, together with well-defined Bragg peaks observed by WAXS on a solid sample, confirm that this polymer is crystallizable and therefore potentially suitable for use as a core-forming block in living CDSA.

By preparing three amphiphilic diBCPs, each with a short PFTMC block and a PEG block of different length, we were able to study the self-assembly behavior of PFTMC containing BCPs in solution. In the case of both PFTMC$_{20}$-*b*-PEG$_{490}$ and PFTMC$_{20}$-*b*-PEG$_{220}$, high aspect ratio fiber-like micelles with lengths predominantly on the order of microns were formed. In contrast, platelet-like micelles were formed from PFTMC$_{20}$-*b*-PEG$_{44}$ which has a significantly shorter corona-forming block. According to the model outlined by Vilgis and Halperin, this micelle morphology is expected to comprise of a chain folded crystalline lamella, sandwiched between two planar layers of solvent swollen corona.[71] This morphology is the thermodynamically most favorable with respect to maximizing the degree of crystallinity of the core-forming block, and minimizing the overall area of the core-solvent interface. By comparison, the increased length of the PEG corona-forming block in PFTMC$_{20}$-*b*-PEG$_{490}$ and PFTMC$_{20}$-*b*-PEG$_{220}$, increases the free energy cost of packing PEG chains around the micelle core. This entropic penalty, caused by corona chain stretching, can be avoided whilst maintaining a platelet morphology by increasing the number of chain folds of the core-forming block and thus decreasing the corona chain density. However, this also increases the area per BCP of the high energy core-solvent interface and incurs a free energy penalty associated with chain folding. Alternatively, the BCPs can adopt a higher aspect ratio fiber-like micelle morphology, where crystallization in the lateral dimension (associated with fiber width) is limited, resulting in a core shape that more closely resembles a narrow ribbon. This reduces the effect of intercoronal steric repulsion as the grafted PEG chains are no longer restricted to a rectangular region of space above a platelet core surface and can now occupy a more expansive region of approximately cylindrical cross-section

9

around the core of the micelles. Using thermodynamic arguments it is therefore possible to conclude that steric repulsion between coronal chains is responsible for the difference in morphology between PFTMC$_{20}$-b-PEG$_{490/220}$ (fibers) and PFTMC$_{20}$-b-PEG$_{44}$ (platelets) presented in this work, and analogous results previously reported for other systems.[8,10,35,74]

However, it is also possible that this phenomenon is a result of a kinetic effect whereby the presence of a longer corona block hinders the lateral growth of the micelle core resulting the observed change from a 2D to a 1D morphology. Two sets of recent results suggest that the change in micelle shape from 2D to 1D caused by an increase in coronal block length can indeed be kinetic in origin. We have previously reported that when the self-assembly of PFS diBCPs with a long corona forming block was performed in a solvent highly selective for the corona the expected 1D fiber-like micelles were formed, whereas when a large fraction of common solvent was present the same block copolymer formed 2D platelets.[65] This morphological difference was attributed to a plasticizing effect of the common solvent on the PFS core, which facilitated more extensive crystallization and lateral growth of the core. More recently, observations by Dove, O'Reilly and coworkers demonstrated a surprising "inverse" effect of block ratio on the morphology of crystalline core BCP micelles.[75] Studies of the formation of di and triBCP micelles with a crystalline PLLA core and a poly(N,N-dimethylacrylamide) corona revealed a morphological preference for 2D platelet micelles over 1D cylinders with increasing percentage composition of the corona-forming block. This remarkable behavior, which is the opposite to that expected based on packing parameter considerations,[3] was attributed to a longer coronal block leading to an increase in the overall solvophilicity of the BCPs and slower self-assembly, thereby resulting in a greater degree of PLLA crystallization and exclusive formation of the platelet morphology.[75,76] These results indicate that a 2D platelet morphology is thermodynamically preferred and that either coronal steric repulsion or low unimer solubility can conspire to yield kinetically trapped 1D assemblies.

Structural Characterization of Fiber-Like PFTMC-b-PEG Micelles. To determine the structure of the crystalline core of the fiber-like PFTMC$_{20}$-b-PEG micelles we combined the insight gained from TEM, AFM, SAXS and WAXS analysis. WAXS analysis of a concentrated solution of PFTMC$_{20}$-b-PEG$_{220}$ micelles revealed Bragg peaks which match three of the peaks observed in the WAXS pattern of PFTMC homopolymer. These results show that the PFTMC segments of these micelles occupy the same crystal lattice as observed for PFTMC homopolymer in its crystalline state. AFM revealed that each micelle has the same height regardless of micelle width, ruling out the possibility of a circularly symmetrical cross-section. This is in agreement with the AFM analysis of PFTMC$_{20}$-b-PEG$_{490}$ seed micelles which could be observed lying on either their largest face or longest edge (Figure **2**). Based on this evidence, we concluded a micelle structure with a rectangular cross-section was present.

A rectangular model was used to fit the SAXS data from a concentrated solution of PFTMC$_{20}$-b-PEG$_{220}$ micelles. This provided a robust fit allowing the average micelle width of these micelles to be determined and the resulting value of 21 nm was reasonable agreement with the widths measured by TEM and AFM. Using the height and width of the micelle core, as determined by SAXS, we were able to calculate the average area of the micelle cross-section. Combining this value with density of PFTMC and M_n of the PFTMC$_{20}$ core-forming block gave a $N_{agg/L}$ of 17 molecules/nm, a value larger than that generally observed for cylindrical micelles with a crystalline PFS core (typically $N_{agg,L}$ = 2-3.5 molecules/nm).[30,77] The comparatively high $N_{agg,L}$ of the PFTMC$_{20}$-b-PEG$_{220}$ micelles studied, can likely be explained by these structures possessing a greater cross-sectional area than typical cylindrical PFS-core micelles (cylindrical micelles with a PFS core typically have a radius of ~4 nm,[70] this corresponds to cross-sectional area of ~50 nm, whereas PFTMC$_{20}$-b-PEG$_{220}$ micelles exhibit a cross-sectional area of ~100 nm) and being comprised of a BCP with a relatively low molecular weight core-forming block with comparable density to PFS (ρ_{PFTMC} = 1.33 g/cm^{-3}, ρ_{PFS} = 1.36 g/cm^{-3}).[78]

Having determined the micelle core dimensions and used molecular mechanics to predict the average length of a PFTMC$_{20}$ chain, we were also able to propose a core structure comprised of PFTMC chains orientated parallel to the height dimension of the core with on average one chain fold as shown in Figure 7. Further structural detail pertaining to the brush density of coronal domains was obtained by allowing the SLD of the corona in Model 2 to refine. A value lower than that of pure PEG homopolymer, but higher than that of the self-assembly solvents (MeOH:DMSO) was obtained, equating to a PEG volume fraction of 0.12±0.01 (see Supporting Information). Based on our proposed chain folded core structure (Figure 7) and given that each PEG chain will possess a solvent swollen coil conformation, it seems likely that the actual volume fraction of PEG chains within the domains defined in Model 2 will be <0.25. This is consistent with the value determined from the refined SLD, and thus supports the plausibility of our proposed structure for PFTMC$_{20}$-b-PEG$_n$ micelles.

Cytotoxicity of Fiber-Like PFTMC-b-PEG Micelles. As a result of the colloidal stability of PFTMC$_{20}$-b-PEG$_{490}$ micelles in water, we were able to investigate the toxicity of these structures towards healthy human cells (WI-38 fetal lung fibroblasts), and the widely studied HeLa cervical cancer cell line. Monodisperse 119 nm (L_w/L_n = 1.04) fiber-like micelles exhibited no significant cytotoxicity at concentrations up to and including 100 µg/mL. Furthermore, whilst the likely metabolite of PFTMC, 9H-fluorene-9,9-dimethanol, does have some cytotoxicity, this was limited to higher concentrations (Figure S19). As PFTMC$_{20}$-b-PEG$_{490}$ is comprised of only ~20 wt% PFTMC, we anticipate that any toxicity of 9H-fluorene-9,9-dimethanol should not present a barrier to most potential biomedical applications.

CONCLUSIONS

In summary, we have reported the first example of monodisperse 1D BCP micelles with a crystalline polycarbonate core. By harnessing the living CDSA of PFTMC, we were able to access low dispersity fiber-like micelles and block comicelles with controlled lengths, ranging from ~40 nm to over 1500 nm. We have also provided a detailed structural analysis of these micelles showing that they possess a rigid rectangular PFTMC core and a solvent swollen PEG corona. This core shape differs from that generally found for fiber-like micelles of PFS, the most well-studied crystallizable polymer used for living CDSA, where a more circular cross-section is normally preferred.[79,80] The rectangular core characteristic of the PFTMC fiber-like micelles leads to the interesting phenomenon where they can lie in two different orientations on a substrate, either on their largest

face or on their edge (Figure 2). As a result of the solubility of PFTMC-*b*-PEG micelles in water, we were able to show that short fiber-like micelles exhibit a lack of any detectable cytotoxicity to both primary and cancerous cells. We also reported the formation of metastable spherical micelles from a fiber-like micelle forming PFTMC-*b*-PEG copolymer. This highlights the opportunity to study the behavior of different micelle morphologies in vivo using this system, without the added complication of concurrently comparing different polymer compositions, as has typically been the case during studies of this kind.[81] The results discussed in this work represent a significant development not only for the field of BCP self-assembly, but also for the larger field of nanomedicine, due to the promising biocompatibility and potential biodegradability of the structures discussed.[59] With this in mind, future work will focus on adapting the coronal chemistry of these micelles for biomedical applications and the study of micelles with alternative crystalline aliphatic polycarbonate cores.

ASSOCIATED CONTENT

Supporting Information

The Supporting Information is available free of charge on the ACS Publications website.

Experimental procedures and additional data (PDF).

AUTHOR INFORMATION

Corresponding Author

*imanners@uvic.ca

Author Contributions

The manuscript was written through contributions of all authors. All authors have given approval to the final version of the manuscript.

ACKNOWLEDGMENT

REFERENCES

(1)   Mai, Y.; Eisenberg, A. Self-Assembly Of Block Copolymers. *Chem. Soc. Rev.* **2012**, *41*, 5969–5985.

(2)   Gröschel, A. H.; Müller, A. H. E. Self-Assembly Concepts For Multicompartment Nanostructures. *Nanoscale* **2015**, *7*, 11841–11876.

(3)   Tritschler, U.; Pearce, S.; Gwyther, J.; Whittell, G. R.; Manners, I. 50th Anniversary Perspective: Functional Nanoparticles From The Solution Self-Assembly Of Block Copolymers. *Macromolecules* **2017**, *50*, 3439–3463.

(4)   Truong, N. P.; Quinn, J. F.; Whittaker, M. R.; Davis, T. P. Polymeric Filomicelles And Nanoworms: Two Decades Of Synthesis And Application. *Polym. Chem.* **2016**, *7*, 4295–4312.

(5)   Li, X.; Wolanin, P. J.; MacFarlane, L. R.; Harniman, R. L.; Qian, J.; Gould, O. E. C.; Dane, T. G.; Rudin, J.; Cryan, M. J.; Schmaltz, T.; Frauenrath, H.; Winnik, M. A.; Faul, C. F. J.; Manners, I. Uniform Electroactive Fibre-Like Micelle Nanowires For Organic Electronics. *Nat. Commun.* **2017**, *8*, 15909.

(6)   Elsabahy, M.; Wooley, K. L. Design Of Polymeric Nanoparticles For Biomedical Delivery Applications. *Chem. Soc. Rev.* **2012**, *41*, 2545–2561.

(7)   Canning, S. L.; Smith, G. N.; Armes, S. P. A Critical Appraisal Of RAFT-Mediated Polymerization-Induced Self-Assembly. *Macromolecules* **2016**, *49*, 1985–2001.

(8)   Cao, L.; Manners, I.; Winnik, M. A. Influence Of The Interplay Of Crystallization And Chain Stretching On Micellar Morphologies: Solution Self-Assembly Of Coil−Crystalline Poly(Isoprene-Block-Ferrocenylsilane). *Macromolecules* **2002**, *35*, 8258–8260.

(9)   He, W. N.; Xu, J. T. Crystallization Assisted Self-Assembly Of Semicrystalline Block Copolymers. *Prog. Polym. Sci.* **2012**, *37*, 1350–1400.

(10)   Massey, J. A.; Temple, K.; Cao, L.; Rharbi, Y.; Raez, J.; Winnik, M. A.; Manners, I. Self-Assembly Of Organometallic Block Copolymers: The Role Of Crystallinity Of The Core-Forming Polyferrocene Block In The Micellar Morphologies Formed By Poly(Ferrocenylsilane-B-Dimethylsiloxane) In N-Alkane Solvents. *J. Am. Chem. Soc.* **2000**, *122*, 11577–11584.

(11)   Petzetakis, N.; Walker, D.; Dove, A. P.; O'Reilly, R. K. Crystallization-Driven Sphere-To-Rod Transition Of Poly(Lactide)-B-Poly(Acrylic Acid) Diblock Copolymers: Mechanism And Kinetics. *Soft Matter* **2012**, *8*, 7408–7414.

(12)   Schmalz, H.; Schmelz, J.; Drechsler, M.; Yuan, J.; Walther, A.; Schweimer, K.; Mihut, A. M. Thermo-Reversible Formation Of Wormlike Micelles With A Microphase-Separated Corona From A Semicrystalline Triblock Terpolymer. *Macromolecules* **2008**, *41*, 3235–3242.

(13)   Surin, M.; Marsitzky, D.; Grimsdale, A. C.; Müllen, K.; Lazzaroni, R.; Leclère, P. Microscopic Morphology Of Polyfluorene–Poly(Ethylene Oxide) Block Copolymers: Influence Of The Block Ratio. *Adv. Funct. Mater.* **2004**, *14*, 708–715.

(14)   Du, Z.-X.; Xu, J.-T.; Fan, Z.-Q. Micellar Morphologies Of Poly(ε-Caprolactone)-B-Poly(Ethylene Oxide) Block Copolymers In Water With A Crystalline Core. *Macromolecules* **2007**, *40*, 7633–7637.

(15)   Lee, C.-U.; Lu, L.; Chen, J.; Garno, J. C.; Zhang, D. Crystallization-Driven Thermoreversible Gelation Of Coil-Crystalline Cyclic And Linear Diblock Copolypeptoids. *ACS Macro Lett.* **2013**, *2*, 436–440.

(16)   Horowitz, G.; Hajlaoui, M. E. Mobility In Polycrystalline Oligothiophene Field-Effect Transistors Dependent On Grain Size. *Adv. Mater.* **2000**, *12*, 1046–1050.

(17)   Crossland, E. J. W.; Tremel, K.; Fischer, F.; Rahimi, K.; Reiter, G.; Steiner, U.; Ludwigs, S. Anisotropic Charge Transport In Spherulitic Poly(3-Hexylthiophene) Films. *Adv. Mater.* **2012**, *24*, 839–844.

(18)   Blanco, E.; Shen, H.; Ferrari, M. Principles Of Nanoparticle Design For Overcoming Biological Barriers To Drug Delivery. *Nat. Biotechnol.* **2015**, *33*, 941–951.

(19)   Geng, Y.; Dalhaimer, P.; Cai, S.; Tsai, R.; Tewari, M.; Minko, T.; Discher, D. E. Shape Effects Of Filaments Versus Spherical Particles In Flow And Drug Delivery. *Nat. Nanotechnol.* **2007**, *2*, 249–255.

(20)   Guérin, G.; Wang, H.; Manners, I.; Winnik, M. A. Fragmentation Of Fiberlike Structures: Sonication Studies Of Cylindrical Block Copolymer Micelles And Behavioral Comparisons To Biological Fibrils. *J. Am. Chem. Soc.* **2008**, *130*, 14763–14771.

(21)   Wang, X.; Guerin, G.; Wang, H.; Wang, Y.; Manners, I.; Winnik, M. A. Cylindrical Block Copolymer Micelles And Co-Micelles Of Controlled Length And Architecture. *Science* **2007**, *317*, 644–647.

(22)   Gilroy, J. B.; Gädt, T.; Whittell, G. R.; Chabanne, L.; Mitchels, J. M.; Richardson, R. M.; Winnik, M. A.; Manners, I.; Gadt, T.; Whittell, G. R.; Chabanne, L.; Mitchels, J. M.; Richardson, R. M.; Winnik, M. A.; Manners, I. Monodisperse Cylindrical Micelles By Crystallization-Driven Living Self-Assembly. *Nat. Chem.* **2010**, *2*, 566–570.

(23)   Kynaston, E. L.; Nazemi, A.; MacFarlane, L. R.; Whittell, G. R.; Faul, C. F. J.; Manners, I. Uniform Polyselenophene Block Copolymer Fiberlike Micelles And Block Co-Micelles Via Living Crystallization-Driven Self-Assembly. *Macromolecules* **2018**, *51*, 1002–1010.

(24) Qian, J.; Lu, Y.; Chia, A.; Zhang, M.; Rupar, P. A.; Gunari, N.; Walker, G. C.; Cambridge, G.; He, F.; Guerin, G.; Manners, I.; Winnik, M. A. Self-Seeding In One Dimension: A Route To Uniform Fiber-Like Nanostructures From Block Copolymers With A Crystallizable Core-Forming Block. *ACS Nano* **2013**, *7*, 3754–3766.

(25) Blundell, D. J.; Keller, A.; Kovacs, A. J. A New Self-Nucleation Phenomenon And Its Application To The Growing Of Polymer Crystals From Solution. *J. Polym. Sci. Part B Polym. Lett.* **1966**, *4*, 481–486.

(26) Hailes, R. L. N.; Oliver, A. M.; Gwyther, J.; Whittell, G. R.; Manners, I. Polyferrocenylsilanes: Synthesis, Properties, And Applications. *Chem. Soc. Rev.* **2016**, *45*, 5358–5407.

(27) Hudson, Z. M.; Lunn, D. J.; Winnik, M. A.; Manners, I. Colour Tunable Fluorescent Multiblock Micelles. *Nat. Commun.* **2014**, *5*, 3372.

(28) He, F.; Gaedt, T.; Manners, I.; Winnik, M. A.; Gädt, T. Fluorescent "Barcode" Multiblock Co-Micelles Via The Living Self-Assembly Of Di- And Triblock Copolymers With A Crystalline Core-Forming Metalloblock. *J. Am. Chem. Soc.* **2011**, *133*, 9095–9103.

(29) Finnegan, J. R.; Lunn, D. J.; Gould, O. E. C.; Hudson, Z. M.; Whittell, G. R.; Winnik, M. A.; Manners, I. Gradient Crystallization-Driven Self-Assembly: Cylindrical Micelles With "Patchy" Segmented Coronas Via The Coassembly Of Linear And Brush Block Copolymers. *J. Am. Chem. Soc.* **2014**, *136*, 13835–13844.

(30) Xu, J.; Zhou, H.; Yu, Q.; Manners, I.; Winnik, M. A. Competitive Self-Assembly Kinetics As A Route To Control The Morphology Of Core-Crystalline Cylindrical Micelles. *J. Am. Chem. Soc.* **2018**, *140*, 2619–2628.

(31) Qiu, H.; Hudson, Z. M.; Winnik, M. A.; Manners, I. Multidimensional Hierarchical Self-Assembly Of Amphiphilic Cylindrical Block Comicelles. *Science* **2015**, *347*, 1329–1332.

(32) Li, X.; Gao, Y.; Boott, C. E.; Hayward, D. W.; Harniman, R.; Whittell, G. R.; Richardson, R. M.; Winnik, M. A.; Manners, I. "Cross" Supermicelles Via The Hierarchical Assembly Of Amphiphilic Cylindrical Triblock Comicelles. *J. Am. Chem. Soc.* **2016**, *138*, 4087–4095.

(33) Tao, D.; Feng, C.; Cui, Y.; Yang, X.; Manners, I.; Winnik, M. A.; Huang, X. Monodisperse Fiber-Like Micelles Of Controlled Length And Composition With An Oligo(P-Phenylenevinylene) Core Via "Living" Crystallization-Driven Self-Assembly. *J. Am. Chem. Soc.* **2017**, *139*, 7136–7139.

(34) Arno, M. C.; Inam, M.; Coe, Z.; Cambridge, G.; Macdougall, L. J.; Keogh, R.; Dove, A. P.; O'Reilly, R. K. Precision Epitaxy For Aqueous 1D And 2D Poly(ε-Caprolactone) Assemblies. *J. Am. Chem. Soc.* **2017**, *139*, 16980–16985.

(35) Robinson, M. E.; Nazemi, A.; Lunn, D. J.; Hayward, D. W.; Boott, C. E.; Hsiao, M.-S.; Harniman, R. L.; Davis, S. A.; Whittell, G. R.; Richardson, R. M.; De Cola, L.; Manners, I. Dimensional Control And Morphological Transformations Of Supramolecular Polymeric Nanofibers Based On Cofacially-Stacked Planar Amphiphilic Platinum(II) Complexes. *ACS Nano* **2017**, *11*, 9162–9175.

(36) Han, L.; Wang, M.; Jia, X.; Chen, W.; Qian, H.; He, F. Uniform Two-Dimensional Square Assemblies From Conjugated Block Copolymers Driven By Π–π Interactions With Controllable Sizes. *Nat. Commun.* **2018**, *9*, 865.

(37) Shin, S.; Menk, F.; Kim, Y.; Lim, J.; Char, K.; Zentel, R.; Choi, T.-L. Living Light-Induced Crystallization-Driven Self-Assembly For Rapid Preparation Of Semiconducting Nanofibers. *J. Am. Chem. Soc.* **2018**, *140*, 6088–6094.

(38) Jin, X.-H.; Price, M. B.; Finnegan, J. R.; Boott, C. E.; Richter, J. M.; Rao, A.; Menke, S. M.; Friend, R. H.; Whittell, G. R.; Manners, I. Long-Range Exciton Transport In Conjugated Polymer Nanofibers Prepared By Seeded Growth. *Science* **2018**, *360*, 897–900.

(39) Petzetakis, N.; Dove, A. P.; O'Reilly, R. K. Cylindrical Micelles From The Living Crystallization-Driven Self-Assembly Of Poly(Lactide)-Containing Block Copolymers. *Chem. Sci.* **2011**, *2*, 955–960.

(40) Zhang, W.; Jin, W.; Fukushima, T.; Saeki, A.; Seki, S.; Aida, T. Supramolecular Linear Heterojunction Composed Of Graphite-Like Semiconducting Nanotubular Segments. *Science* **2011**, *334*, 340–343.

(41) Schmelz, J.; Schedl, A. E.; Steinlein, C.; Manners, I.; Schmalz, H. Length Control And Block-Type Architectures In Worm-Like Micelles With Polyethylene Cores. *J. Am. Chem. Soc.* **2012**, *134*, 14217–14225.

(42) Qian, J.; Li, X.; Lunn, D. J.; Gwyther, J.; Hudson, Z. M.; Kynaston, E.; Rupar, P. A.; Winnik, M. A.; Manners, I. Uniform, High Aspect Ratio Fiber-Like Micelles And Block Co-Micelles With A Crystalline π-Conjugated Polythiophene Core By Self-Seeding. *J. Am. Chem. Soc.* **2014**, *136*, 4121–4124.

(43) Ogi, S.; Sugiyasu, K.; Manna, S.; Samitsu, S.; Takeuchi, M. Living Supramolecular Polymerization Realized Through A Biomimetic Approach. *Nat. Chem.* **2014**, *6*, 188–195.

(44) Robinson, M. E.; Lunn, D. J.; Nazemi, A.; Whittell, G. R.; De Cola, L.; Manners, I. Length Control Of Supramolecular Polymeric Nanofibers Based On Stacked Planar Platinum(II) Complexes By Seeded-Growth. *Chem. Commun.* **2015**, *51*, 15921–15924.

(45) Li, X.; Jin, B.; Gao, Y.; Hayward, D. W.; Winnik, M. A.; Luo, Y.; Manners, I. Monodisperse Cylindrical Micelles Of Controlled Length With A Liquid-Crystalline Perfluorinated Core By 1D "Self-Seeding." *Angew. Chemie - Int. Ed.* **2016**, *55*, 11392–11396.

(46) Schöbel, J.; Burgard, M.; Hils, C.; Dersch, R.; Dulle, M.; Volk, K.; Karg, M.; Greiner, A.; Schmalz, H. Bottom-Up Meets Top-Down: Patchy Hybrid Nonwovens As An Efficient Catalysis Platform. *Angew. Chemie - Int. Ed.* **2017**, *56*, 405–408.

(47) Bruckman, M. A.; Randolph, L. N.; VanMeter, A.; Hern, S.; Shoffstall, A. J.; Taurog, R. E.; Steinmetz, N. F. Biodistribution, Pharmacokinetics, And Blood Compatibility Of Native And PEGylated Tobacco Mosaic Virus Nano-Rods And -Spheres In Mice. *Virology* **2014**, *449*, 163–173.

(48) Nazemi, A.; Boott, C. E.; Lunn, D. J.; Gwyther, J.; Hayward, D. W.; Richardson, R. M.; Winnik, M. A.; Manners, I. Monodisperse Cylindrical Micelles And Block Comicelles Of Controlled Length In Aqueous Media. *J. Am. Chem. Soc.* **2016**, *138*, 4484–4493.

(49) He, W.-N.; Zhou, B.; Xu, J.-T.; Du, B.-Y.; Fan, Z.-Q. Two Growth Modes Of Semicrystalline Cylindrical Poly(ε-Caprolactone)-B-Poly(Ethylene Oxide) Micelles. *Macromolecules* **2012**, *45*, 9768–9778.

(50) Sun, L.; Petzetakis, N.; Pitto-Barry, A.; Schiller, T. L.; Kirby, N.; Keddie, D. J.; Boyd, B. J.; O'Reilly, R. K.; Dove, A. P. Tuning The Size Of Cylindrical Micelles From Poly(L-Lactide)-B-Poly(Acrylic Acid) Diblock Copolymers Based On Crystallization-Driven Self-Assembly. *Macromolecules* **2013**, *46*, 9074–9082.

(51) Pitto-Barry, A.; Kirby, N.; Dove, A. P.; O'Reilly, R. K. Expanding The Scope Of The Crystallization-Driven Self-Assembly Of Polylactide-Containing Polymers. *Polym. Chem.* **2014**, *5*, 1427–1436.

(52) Song, Y.; Chen, Y.; Su, L.; Li, R.; Letteri, R. A.; Wooley, K. L. Crystallization-Driven Assembly Of Fully Degradable, Natural Product-Based Poly(L-Lactide)-Block-Poly(α-D-Glucose Carbonate)S In Aqueous Solution. *Polymer* **2017**, *122*, 270–279.

(53) Pêgo, A. P.; Grijpma, D. W.; Feijen, J. Enhanced Mechanical Properties Of 1,3-Trimethylene Carbonate Polymers And Networks. *Polymer* **2003**, *44*, 6495–6504.

(54) Zhu, K. J.; Hendren, R. W.; Jensen, K.; Pitt, C. G. Synthesis, Properties, And Biodegradation Of Poly(1,3-Trimethylene Carbonate). *Macromolecules* **1991**, *24*, 1736–1740.

(55) Vene, E.; Barouti, G.; Jarnouen, K.; Gicquel, T.; Rauch, C.; Ribault, C.; Guillaume, S. M.; Cammas-Marion, S.; Loyer, P. Opsonisation Of Nanoparticles Prepared From Poly(β-Hydroxybutyrate) And Poly(Trimethylene Carbonate)-B-Poly(Malic Acid) Amphiphilic Diblock Copolymers: Impact On The In Vitro Cell Uptake By Primary Human Macrophages And HepaRG Hepatoma Cells. *Int. J. Pharm.* **2016**, *513*, 438–452.

(56) Yang, L. Q.; He, B.; Meng, S.; Zhang, J. Z.; Li, M.; Guo, J.; Guan, Y. M.; Li, J. X.; Gu, Z. W. Biodegradable Cross-Linked Poly(Trimethylene Carbonate) Networks For Implant Applications: Synthesis And Properties. *Polymer* **2013**, *54*, 2668–2675.

(57) Nederberg, F.; Zhang, Y.; Tan, J. P. K.; Xu, K.; Wang, H.; Yang, C.; Gao, S.; Guo, X. D.; Fukushima, K.; Li, L.; Hedrick, J. L.; Yang, Y. Y. Biodegradable Nanostructures With Selective Lysis Of Microbial Membranes. *Nat. Chem.* **2011**, *3*, 409–414.

(58) Brannigan, R. P.; Dove, A. P. Synthesis, Properties And Biomedical Applications Of Hydrolytically Degradable Materials Based On Aliphatic Polyesters And Polycarbonates. *Biomater. Sci.* **2017**, *5*, 9–21.

(59) Zhang, Z.; Kuijer, R.; Bulstra, S. K.; Grijpma, D. W.; Feijen, J. The In Vivo And In Vitro Degradation Behavior Of Poly(Trimethylene Carbonate). *Biomaterials* **2006**, *27*, 1741–1748.

(60) Nederberg, F.; Lohmeijer, B. G. G.; Leibfarth, F.; Pratt, R. C.; Choi, J.; Dove, A. P.; Waymouth, R. M.; Hedrick, J. L. Organocatalytic Ring Opening Polymerization Of Trimethylene Carbonate. *Biomacromolecules* **2007**, *8*, 153–160.

(61) Venkataraman, S.; Hedrick, J. L.; Yang, Y. Y. Fluorene-Functionalized Aliphatic Polycarbonates: Design, Synthesis And Aqueous Self-Assembly Of Amphiphilic Block Copolymers. *Polym. Chem.* **2014**, *5*, 2035–2040.

(62) Dove, A. P. Organic Catalysis For Ring-Opening Polymerization. *ACS Macro Lett.* **2012**, *1*, 1409–1412.

(63) Lammertink, R. G. H.; Hempenius, M. A.; Manners, I.; Vancso, G. J. Crystallization And Melting Behavior Of Poly(Ferrocenyldimethylsilanes) Obtained By Anionic Polymerization. *Macromolecules* **1998**, *31*, 795–800.

(64) Pope, D. P. Characterization Of Oriented Low-Density Polyethylene Samples By Differential Scanning Calorimetry. *J. Polym. Sci. Polym. Phys. Ed.* **1976**, *14*, 811–820.

(65) Hsiao, M.; Yusoff, S. F. M.; Winnik, M. A.; Manners, I. Crystallization-Driven Self-Assembly Of Block Copolymers With A Short Crystallizable Core-Forming Segment: Controlling Micelle Morphology Through The Influence Of Molar Mass And Solvent Selectivity. *Macromolecules* **2014**, *47*, 2361–2372.

(66) Shen, L.; Wang, H.; Guerin, G.; Wu, C.; Manners, I.; Winnik, M. A. A Micellar Sphere-To-Cylinder Transition Of Poly(Ferrocenyldimethylsilane-B-2-Vinylpyridine) In A Selective Solvent Driven By Crystallization. *Macromolecules* **2008**, *41*, 4380–4389.

(67) Wang, H.; Winnik, M. A.; Manners, I. Synthesis And Self-Assembly Of Poly(Ferrocenyldimethylsilane-B-2-Vinylpyridine) Diblock Copolymers. *Macromolecules* **2007**, *40*, 3784–3789.

(68) de Jeu, W. H. Basic X-Ray Scattering For Soft Matter. *Basic X-ray Scattering for Soft Matter*; Oxford University Press, 2016.

(69) Zemb, T.; Lindner, P. Neutron, X-Rays And Light. Scattering Methods Applied To Soft Condensed Matter. *Neutron, X-rays and Light. Scattering Methods Applied to Soft Condensed Matter*; 1st ed.; Elsevier, 2002.

(70) Hayward, D. W.; Gilroy, J. B.; Rupar, P. A.; Chabanne, L.; Pizzey, C.; Winnik, M. A.; Whittell, G. R.; Manners, I.; Richardson, R. M. Liquid Crystalline Phase Behavior Of Well-Defined Cylindrical Block Copolymer Micelles Using Synchrotron Small-Angle X-Ray Scattering. *Macromolecules* **2015**, *48*, 1579–1591.

(71) Vilgis, T.; Halperin, A. Aggregation Of Coil-Crystalline Block Copolymers: Equilibrium Crystallization. *Macromolecules* **1991**, *24*, 2090–2095.

(72) Nakazono, K.; Yamashita, C.; Ogawa, T.; Iguchi, H.; Takata, T. Synthesis And Properties Of Pendant Fluorene Moiety-Tethered Aliphatic Polycarbonates. *Polym. J.* **2015**, *47*, 355–361.

(73) Gao, Y.; Qiu, H.; Zhou, H.; Li, X.; Harniman, R.; Winnik, M. A.; Manners, I. Crystallization-Driven Solution Self-Assembly Of Block Copolymers With A Photocleavable Junction. *J. Am. Chem. Soc.* **2015**, *137*, 2203–2206.

(74) Du, Z. X.; Xu, J. T.; Fan, Z. Q. Micellar Morphologies Of Poly(ε-Caprolactone)-B-Poly(Ethylene Oxide) Block Copolymers In Water With A Crystalline Core. *Macromolecules* **2007**, *40*, 7633–7637.

(75) Yu, W.; Inam, M.; Jones, J. R.; Dove, A. P.; O'Reilly, R. K. Understanding The CDSA Of Poly(Lactide) Containing Triblock Copolymers. *Polym. Chem.* **2017**, *8*, 5504–5512.

(76) Inam, M.; Cambridge, G.; Pitto-Barry, A.; Laker, Z. P. L.; Wilson, N. R.; Mathers, R. T.; Dove, A. P.; O'Reilly, R. K. 1D Vs. 2D Shape Selectivity In The Crystallization-Driven Self-Assembly Of Polylactide Block Copolymers. *Chem. Sci.* **2017**, *8*, 4223–4230.

(77) Cambridge, G.; Guerin, G.; Manners, I.; Winnik, M. A. Fiberlike Micelles Formed By Living Epitaxial Growth From Blends Of Polyferrocenylsilane Block Copolymers. *Macromol. Rapid Commun.* **2010**, *31*, 934–938.

(78) Whittell, G. R.; Gilroy, J. B.; Grillo, I.; Manners, I.; Richardson, R. M. The Solution Phase Characterization Of Poly(Ferrocenyldimethylsilane)S By Small-Angle Neutron Scattering. *J. Polym. Sci. Part A Polym. Chem.* **2013**, *51*, 4011–4020.

(79) Gilroy, J. B.; Rupar, P. A.; Whittell, G. R.; Chabanne, L.; Terrill, N. J.; Winnik, M. A.; Manners, I.; Richardson, R. M. Probing The Structure Of The Crystalline Core Of Field-Aligned, Monodisperse, Cylindrical Polyisoprene-Block-Polyferrocenylsilane Micelles In Solution Using Synchrotron Small- And Wide-Angle X-Ray Scattering. *J. Am. Chem. Soc.* **2011**, *133*, 17056–17062.

(80) Qiu, H.; Gao, Y.; Du, V. A.; Harniman, R.; Winnik, M. a.; Manners, I. Branched Micelles By Living Crystallization-Driven Block Copolymer Self-Assembly Under Kinetic Control. *J. Am. Chem. Soc.* **2015**, *137*, 2375–2385.

(81) Kaga, S.; Truong, N. P.; Esser, L.; Senyschyn, D.; Sanyal, A.; Sanyal, R.; Quinn, J. F.; Davis, T. P.; Kaminskas, L. M.; Whittaker, M. R. Influence Of Size And Shape On The Biodistribution Of Nanoparticles Prepared By Polymerization-Induced Self-Assembly. *Biomacromolecules* **2017**, *18*, 3963–3970.